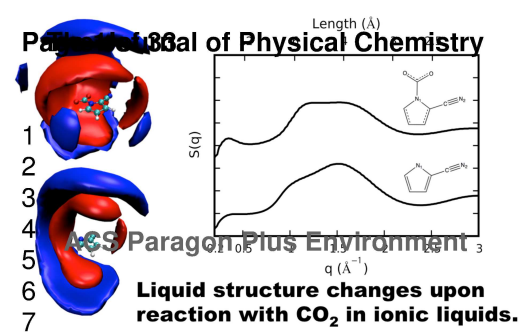
The Journal of Physical Chemistry

This document is confidential and is proprietary to the American Chemical Society and its authors. Do not copy or disclose without written permission. If you have received this item in error, notify the sender and delete all copies.

Liquid Structure of CO₂-Reactive Aprotic Heterocyclic Anion Ionic Liquids from X-Ray Scattering and Molecular Dynamics

Journal:	The Journal of Physical Chemistry		
Manuscript ID	jp-2016-07713k.R1		
Manuscript Type:	Article		
Date Submitted by the Author:	07-Oct-2016		
Complete List of Authors:	Sheridan, Quintin; University of Notre Dame, Chemical and Biomolecular Engineering Oh, Seungmin; University of Notre Dame, Chemical and Biomolecular Engineering Morales-Collazo, Oscar; University of Notre Dame, Dept. of Chemical and Biomolecular Engineering Castner, Edward; Rutgers, The State University of New Jersey, Department of Chemistry and Chemical Biology Brennecke, Joan; University of Notre Dame, Dept. of Chemical and Biomolecular Engineering Maginn, Edward; University of Notre Dame, Department of Chemical Engineering		

SCHOLARONE™ Manuscripts



Liquid Structure of CO₂-Reactive Aprotic Heterocyclic Anion Ionic Liquids from X-ray Scattering and Molecular Dynamics

Quintin R. Sheridan[†], Seungmin Oh[†], Oscar Morales-Collazo[†],

Edward W. Castner,Jr.[‡], Joan F. Brennecke[†], Edward J. Maginn^{††}

[†]Department of Chemical and Biomolecular Engineering

University of Notre Dame

Notre Dame, Indiana, 46556

[‡]Department of Chemistry and Chemical Biology

Rutgers, The State University of New Jersey

New Brunswick, New Jersey 08901

October 5, 2016

^{*}jfb@nd.edu $\dagger ed@nd.edu$

Abstract

A combination of X-ray scattering experiments and molecular dynamics simulations were conducted to investigate the structure of ionic liquids (ILs) which chemically bind CO₂. The structure functions were measured and computed for four different ILs consisting of two different phosphonium cations, triethyloctylphosphonium ($[P_{2228}]^+$) and trihexyltetradecylphosphonium ([P₆₆₆₁₄]⁺), paired with two different aprotic heterocyclic anions which chemically react with CO₂, 2-cyanopyrrolide and 1,2,4-triazolide. Simulations were able to reproduce the experimental structure functions, and by deconstructing the simulated structure functions, further information on the liquid structure was obtained. All structure functions of the ILs studied had three primary features which have been seen before in other ILs: a prepeak near $0.3\text{-}0.4~\text{Å}^{-1}$ corresponding to polar/nonpolar domain alternation, a charge alternation peak near 0.8 Å^{-1} , and a peak near 1.5 ${\rm \AA}^{-1}$ due to interactions of adjacent molecules. The liquid structure functions were only mildly sensitive to the specific anion and whether or not they were reacted with CO₂. Upon reacting with CO₂, small changes were observed in the structure functions of the $[P_{2228}]^+$ ILs, whereas virtually no change was observed upon reacting with CO_2 in the corresponding $[P_{66614}]^+$ ILs. When the $[P_{2228}]^+$ cation was replaced with the $[P_{66614}]^+$ cation, there was a significant increase in the intensities of the prepeak and adjacency interaction peak. While many of the liquid structure functions are similar, the actual liquid structures differ as demonstrated by computed spatial distribution functions.

1 Introduction

Ionic liquids (ILs) have gained considerable attention as solvents capable of outperforming current amine technologies in CO₂ capture. ^{1–3} ILs have several unique properties such as low vapor pressure, high thermal stability, and high chemical stability. These properties provide practical advantages over amines, which are volatile and corrosive. Recently, a class of ILs with aprotic heterocyclic anions (AHAs) were developed that chemically bind CO₂ without showing a dramatic increase in viscosity. ^{4–7} Although much is known about the physical and chemical properties of these ILs, little is known about their liquid structure.

Several research groups have examined the liquid structure for other classes of ILs using X-ray or neutron scattering experiments combined with molecular dynamics (MD) simulations. 8-18 A number of groups have used high-energy X-ray scattering experiments to study the liquid structure for a variety of ILs with different types of anions and cations. 13,15,19-23 The electrostatic interactions that dominate the liquid ordering typically result in three primary long range structure function features: a prepeak also known as a first sharp diffraction peak between $0.25-0.5 \text{ Å}^{-1}$ due to the alternation of polar/nonpolar domains, a charge separation feature near 1 $Å^{-1}$, and a peak near 1.5 $Å^{-1}$ due to adjacency interactions within the IL. The prepeak is usually attributed to heterogeneous domain formation within the IL, which generally requires ions of sufficient size with long nonpolar tails although this is not always the case. ^{13,16,19–22,24–31} Several computational researchers have demonstrated that MD simulations can recover the experimental structure functions and shed light on the specific molecular correlations responsible for these features. 9,17,31-36 Partitioning of the total structure function into partial structure functions representing the correlations between the different ions revealed a charge alternation feature, which was absent in the total structure function of certain ILs due to the cancellation of peaks and antipeaks. Kashyap found that when the long alkyl cation tails are functionalized with polar ether groups, the liquid structure function changes dramatically and the prepeak disappears.³³ Additionally, simulations showed the percolation of polar and nonpolar networks that are primarily responsible for the ordering within ILs. 8,9,17,23,29,33,36

The objective of the present work is to obtain a detailed understanding of the liquid

structure of AHA ILs in both the unreacted and CO_2 -reacted states using a combination of X-ray scattering experiments and MD simulations. The ILs studied are a combination of two phosphonium cations, triethyloctylphosphonium ($[P_{2228}]^+$) and trihexyltetradecylphosphonium ($[P_{66614}]^+$), paired with two different AHA anions, 2-cyanopyrrolide ($[2CNpyr]^-$) and 1,2,4-triazolide ($[4Triaz]^-$). These ILs have shown great promise as CO_2 capture solvents. The effects of the CO_2 reaction on the liquid structure are investigated by comparison of neat and CO_2 complexed IL structure functions. Additionally, we examine the changes in the IL structure from both cation and anion substitutions. Finally we comment on the ability of the structure function to describe the liquid structure and the additional insights provided by MD simulation.

2 Experimental Methods

2.1 Material Synthesis

Triethylphosphine (99% purity), 1-bromooctane (99% purity), and 1H-1,2,4-triazole (98% purity) were purchased from Sigma-Aldrich, trihexyl(tetradecyl)phosphonium bromide (95% purity) was purchased from Strem Chemicals, 1H-pyrrole-2-carbonitrile (99% purity) and Amberlite IRN78 (nuclear grade) were purchased from Alfa Aesar, and anhydrous toluene (99.8% purity) was purchased from EDM. All chemicals were used without further purification.

$[\mathbf{P}_{2228}][\mathbf{Br}]$

Under a nitrogen atmosphere and in a flame dried round bottom flask (500 mL), a solution of triethylphosphine (25 g, 212 mmol) in anhydrous toluene (200 mL) was treated with 1-bromooctane (43 g, 222 mmol) via cannula. The solution was stirred at room temperature for 20 minutes and at 70 °C for 5 hours. After completion, the reaction product was concentrated, dissolved in acetonitrile, and recrystallized from acetonitrile/ethyl acetate (1:2) to obtain [P₂₂₂₈][Br] as a white solid.

$[P_{2228}][2CNpyr]$

In a round bottom flask (500 mL), a solution of triethyloctylphosphonium bromide ([P₂₂₂₈][Br]) (10 g, 32.1 mmol) in methanol (200 mL) was treated with Amberlite IRN78 (93 g) and mixed until no residual halide precipitation was observed by AgNO₃ test to obtain [P₂₂₂₈][OH]. The mixture was filtered and treated with 1H-pyrrole-2-carbonitrile (2.21 g, 32.1 mmol) and stirred for 2 days.

$[P_{2228}][4Triaz]$

The reaction was performed per the above synthesis of $[P_{2228}][2CNpyr]$, but with 1H-1,2,4-triazole (2.96 g, 32.1 mmol), and stirred for 2 days.

$[P_{66614}][2CNpyr]$

The reaction was performed per the above synthesis of $[P_{2228}][2CNpyr]$, but with $[P_{66614}][Br]$ and 1H-pyrrole-2-carbonitrile (1.634 g, 17.74 mmol), and stirred for 2 days.

$[\mathbf{P}_{66614}][\mathbf{4Triaz}]$

The reaction was performed per the above synthesis of $[P_{2228}][2CNpyr]$, but with $[P_{66614}][Br]$ and 1H-1,2,4-triazole (1.225 g, 17.74 mmol), and stirred for 2 days.

Methanol and other volatiles were removed at 323.15 K under reduced pressure (10 mbar). Complete removal of volatiles was confirmed by ¹H NMR. The water byproduct was then removed by further drying at 323.15 K under reduced pressure for approximately 3 days. The water content of each IL was determined by a Metrohm 831 Karl Fischer coulometer and was less than 0.05% by weight (or 500 ppm). The structures of the ILs were verified by ¹H NMR (Varian INOVA-600) spectroscopy with dried ILs dissolved in deuterated dimethyl sulfoxide (DMSO-d6, 99.9 atom %D, Sigma-Aldrich) containing 1% v/v TMS. Any residual halide in the aqueous phase in contact with the ILs was not detectable on addition of aqueous AgNO₃.

2.2 Density Measurements

IL densities were measured in the temperature range of 10 to 80 °C for pure ILs and 10 to 30 °C for CO₂ saturated ILs using a DMA 4500 Anton Paar oscillating U-tube densitometer (\pm 0.01 °C, \pm 1 x 10⁻³ g cm⁻³). Approximately 1.5 mL of IL was prepared in a nitrogen-filled glove box and loaded into the densitometer.

2.3 CO₂ Saturation

IL samples of approximately 2 g were saturated with CO₂ at room temperature (22 °C) and approximately 1.3 bar CO₂ pressure using a reactor (235 mL) and a CO₂ reservoir (290 mL). Absorption of water and CO₂ from the atmosphere was prevented by keeping the apparatus and sample vessel completely sealed and by preparing and loading the samples in a nitrogenfilled glove box. The reactor was initially evacuated for approximately 30 minutes with a Welch Gem 8890 model vacuum pump, and CO₂ was briefly introduced several times and the mixture was stirred with a magnetic stir-bar until equilibrium was reached at approximately 1.3 bar. Because the volume of the system was controlled during the CO₂ saturation, the vapor-liquid equilibrium point was determined after the pressure remained constant for at least 2 hours. The CO₂ solubility for the [P₂₂₂₈][4Triaz] was determined volumetrically as described in previous work.⁵

2.4 Water Content Measurements

The water content was measured both before and after CO_2 saturation and density measurements using a Metrohm 831 Karl Fischer coulometer with \pm 3 μ g water resolution. The water contents were less than 500 ppm both before and after the measurements.

2.5 X-ray Scattering Experiments

X-ray scattering data was obtained in a momentum transfer (q) range of 0.2 to 20 Å⁻¹ using X-rays generated at the Advanced Photon Source (APS) beam-line 11-ID-B at Argonne National Laboratory. As mentioned above, all samples contained less than 500 ppm of water for

both pure and CO_2 saturated ILs. All IL structure functions were measured at room temperature where the ILs remained liquid (note that $[P_{2228}][4\text{Triaz}]$ was a super-cooled liquid). Each sample was transferred into a 2 mm quartz capillary (HR6-150, Hampton Research) in a nitrogen-filled glove box and flame sealed after evacuation of the air inside. Samples were exposed to a collimated X-ray beam (58.65 kV, $\lambda = 0.2114$ Å) with a monochromator of Si(311), a beam size of 0.5 mm x 0.5 mm and a 120 s total exposure time. A Perkin 1621-104 CN3-EHS Elmer amorphous silicon detector measured the X-ray scattering patterns. The given X-ray scattering data were post-processed for integration and domain conversion from scattering angle, 2Θ , to scattering vector, q, using the Fit2D software package from Hammersley et al. ^{37,38} The total structure function was calculated using eq. 1

$$S(q) = \frac{I_{coh}(q) - \sum_{i} x_{i} f_{i}^{2}(q)}{\left[\sum_{i} x_{i} f_{i}^{2}(q)\right]^{2}}$$
(1)

in which $I_{coh}(q)$ indicates the total intensity, x_i is fraction of atom type i, and $f_i(q)$ is the atomic form factor of atom type i found in the International Tables of Crystallography.³⁹ The structure function calculation and various corrections were processed using PDFgetX2 software from Qui *et al.*⁴⁰ The atomic fraction of each CO₂ saturated IL was determined using previously reported and new experimental CO₂ solubility data: 0.92, 0.9, 0.8, and 0.8 moles of CO₂ per mole IL for $[P_{2228}][2CNpyr]^5$, $[P_{66614}][2CNpyr]^4$, $[P_{2228}][4Triaz]$, and $[P_{66614}][4Triaz]^4$, respectively.

3 Computational Methods

The structures of the ions studied in this work are shown in Figure 1. [4Triaz]⁻ has two different nitrogen sites where the CO₂ can react. It is currently unknown where the [4Triaz]⁻ reaction site is in the liquid phase. Therefore, both reaction sites were considered in this work with the hope that comparison of the simulated and experimental structure functions would identify the stable reaction site.

$$\begin{array}{c} \overset{\text{CH}_3}{(\text{CH}_2)_m} \\ \overset{\text{CH}_3}{(\text{CH}_2)_m} \\ \overset{\text{CH}_3}{(\text{CH}_2)_m} - \overset{\text{P}}{P} - (\text{CH}_2)_n - \text{CH}_3 \\ \overset{\text{CH}_3}{(\text{CH}_2)_m} & \text{m} = 1, 5 \\ \overset{\text{CH}_3}{(\text{CH}_3)_m} & \text{n} = 7, 13 \end{array}$$

$$\begin{array}{c} \overset{\text{N}_1}{(\text{CH}_2)_m} & \overset{\text{N}_2}{(\text{CH}_2)_m} \\ \overset{\text{C}}{(\text{CH}_2)_m} & \text{m} = 1, 5 \\ \overset{\text{C}}{(\text{CH}_3)_m} & \text{n} = 7, 13 \end{array}$$

$$\begin{array}{c} \overset{\text{N}_2}{(\text{CH}_2)_m} & \overset{\text{N}_2}{(\text{CH}_2)_m} \\ \overset{\text{C}}{(\text{CH}_2)_m} & \text{m} = 1, 5 \\ \overset{\text{C}}{(\text{CH}_2)_m} & \text{n} = 7, 13 \end{array}$$

$$\begin{array}{c} \overset{\text{N}_2}{(\text{CH}_2)_m} & \overset{\text{N}_2}{(\text{CH}_2)_m} \\ \overset{\text{N}_3}{(\text{CH}_3)_m} & \overset{\text{N}_2}{(\text{CH}_2)_m} \\ \overset{\text{N}_3}{(\text{CH}_2)_m} & \overset{\text{N}_3}{(\text{CH}_2)_m} & \overset{\text{N}_3}{(\text{CH}_2)_m} \\ \overset{\text{N}_3}{(\text{CH}_2)_m} & \overset{\text{N}_3}{(\text{CH}_2)_m} & \overset{\text{N}_3}{(\text{CH}_2)_m} \\ \overset{\text{N}_3}{(\text{CH}_2)_m} & \overset{\text{N}_3}{(\text{CH}_2)_m} & \overset{\text{N}_3}{(\text{CH}_2)_m} & \overset{\text{N}_3}{(\text{CH}_2)_m} & \overset{\text{N}_3}{(\text{CH}_2)_m} \\ \overset{\text{N}_3}{(\text{CH}_2)_m} & \overset{\text{N}_3}{(\text{CH$$

Figure 1: Structures of ions studied in this work. The phosphonium cations have different alkyl chain lengths where m and n are equal to 1 and 7 or 5 and 13 for $[P_{2228}]^+$ and $[P_{66614}]^+$, respectively.

The liquid structure function was calculated via MD simulations using eq. 2

$$S(q) = \frac{\rho_0 \sum_{i=1}^{N} \sum_{j=1}^{N} x_i f_i(q) x_j f_j(q) \int_0^{r_\infty} 4\pi r^2 (g_{ij}(r) - 1) \frac{\sin(qr)}{qr} W(r) dr}{\left[\sum_{i=1}^{N} x_i f_i(q)\right]^2}$$
(2)

where S(q) is the total structure function, ρ_o is the atomic number density, i and j are indices for unique atom types, N is the total number of atom types, $f_i(q)$ is the atomic form factor for atom type i, $g_{ij}(r)$ is the pair distribution function between atoms of types i and j, r is the distance between atoms i and j, and q is the scattering vector. W(r) is a Lorch window function given by $W(r) = \sin(2\pi r/L)/(2\pi r/L)$. ³⁶ Computer simulations can provide additional understanding of experimental structure functions because the summation limits in eq. 2 can be selected to extract partial structure functions correlating specific groups of atoms. For example, both summations can run over the indices of cation atoms thereby obtaining the cation-cation contribution to the total structure function. By partitioning the total structure function in this way, one can gain valuable insights into the interactions which determine the liquid structure. Previous works by Santos and Kashyap showed that this partitioning reveals important features of the liquid structure which can remain absent in the experimental structure function due to the cancellation of peaks by antipeaks. ^{15,32–34}

To calculate the liquid structure functions, a series of MD simulations were run using GROMACS version 4.5.5. 41–43 Initial structures were generated by placing 1000-2000 ion ACS Paragon Plus Environment

pairs in a simulation box using Packmol. 44 In modeling the CO₂-reacted ILs, it was assumed that all of the anions were bound to CO₂. No physically absorbed CO₂ was considered as the amount of physically absorbed CO_2 is estimated to be less than 3 mole $\%.^5$ Next, a steepest descent energy minimization was performed. Following the energy minimization, the systems were annealed to 700 K for 500 ps, and subsequently equilibrated in the NPT ensemble. The equilibration procedure differed depending on the system due to the large size and slow dynamics of the $[P_{66614}]^+$ cation. Production runs for systems with $[2CNpyr]^$ were run at 300 K while production runs for systems with [4Triaz] were run at 313 K due to the higher melting point of ILs with this anion. Note that the temperature difference of 18 K between the simulations and experiments will have a negligible impact on the liquid structure functions due to the low thermal expansivities of ILs. 15,35 For the $[P_{2228}]^+$ systems, an initial NPT equilibration to the production temperature and 1 atm was performed for 8 ns using a Berendsen thermostat and barostat. Next, the systems were equilibrated for an additional 2 ns using a Nosé-Hoover thermostat 45,46 and a Parinello-Rahman barostat. 47 Following the equilibration, an NVT production run of 2-4 ns was performed, saving configurations every 0.1-0.3 ps. For the $[P_{66614}]^+$ systems, additional initial equilibration was performed to allow the system to relax properly following the annealing. For these systems, the temperature was decreased by 100 K over 1 ns intervals until reaching the production temperature. At this point the same equilibration and production run procedures of the $[P_{2228}]^+$ systems were followed. For all simulations, a time step of 1 fs was used. All covalent bonds to hydrogen were constrained using the LINCS algorithm to allow a larger time step. 48 The equations of motion were integrated using the Verlet Leap-Frog algorithm. 49,50 Long range electrostatics were handled using particle-mesh Ewald summation.⁵¹ Long range corrections were applied to both energy and pressure. Lorentz-Berthelot mixing rules were applied to Lennard-Jones interactions. 52 A description of the force field parameterization and all force field parameters are provided in the supporting information (SI).

Preliminary simulations were performed on the [P₂₂₂₈][2CNpyr] system to evaluate the effects of the cutoff radius as well as the system size on the calculated structure function. First, simulations of 1000 ion pairs were run where the cutoff radius was set to either 12 or 14 Å. The resulting structure functions were found to be unaffected by an increase in the ACS Paragon Plus Environment

cutoff radius. Therefore, the cutoff was set to 12 Å for all remaining systems to speed up the simulations. The system size was then tested by performing simulations of 1000 and 2000 ion pairs. Again these simulations produced nearly identical structure functions so all further simulations used between 1000 and 2000 ion pairs. The structure functions resulting from the different systems sizes and cutoff radii are shown in the SI.

4 Results

4.1 Experimental Structure Functions

The experimental structure functions are shown in Figure 2 for ILs containing $[P_{2228}]^+$ with unreacted and CO_2 -reacted $[2CNpyr]^-$ and $[4Triaz]^-$. For the unreacted $[4Triaz]^-$, there is a small prepeak at 0.42 Å^{-1} and two additional overlapping peaks near 1 Å^{-1} and 1.5 Å^{-1} . The unreacted $[2CNpyr]^-$ has the same overlapping peaks near 1 Å^{-1} and 1.5 Å^{-1} , but it does not have a clearly defined prepeak. For the CO_2 -reacted ILs, the overlapping peaks at 1.5 Å^{-1} become more pronounced for $[2CNpyr]^-$, but for $[4Triaz]^-$ there is only one peak. The prepeaks are still present for the CO_2 -reacted ILs, with the one for $[2CNpyr]^-$ becoming more pronounced upon reaction. Previous studies on other ILs have observed these three peaks, assigning them as a prepeak, a charge alternation peak, and an adjacency peak, respectively. $^{15,32-34}$ In the intra-molecular region $(q > 2 \text{ Å}^{-1})$, the structure functions of all liquids are similar because the cations are the same and the anions have very similar structures.

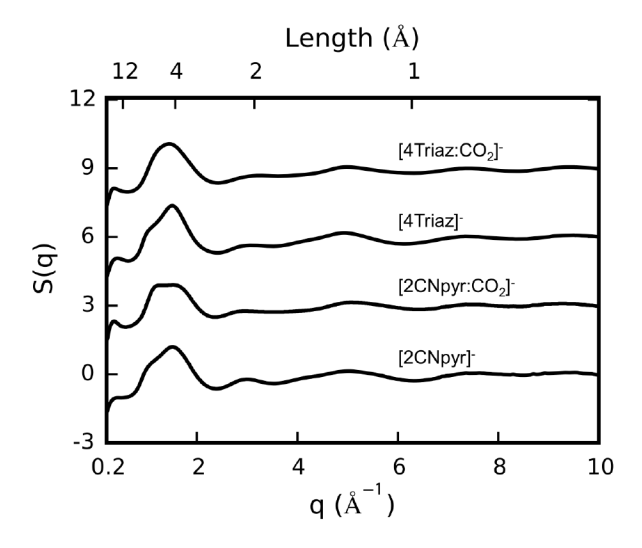


Figure 2: Room temperature (295 K) experimental structure functions for all ILs with $[P_{2228}]^+$. The structure functions are offset by 0, 3, 6, and 9 for $[2CNpyr]^-$, $[2CNpyr:CO_2]^-$, $[4Triaz]^-$, and $[4Triaz:CO_2]^-$, respectively. The primary abscissa (bottom) is in reciprocal space while the secondary abscissa (top) shows the corresponding real space distance.

Figure 3 compares the experimental structure functions for unreacted and CO₂-reacted $[2\text{CNpyr}]^-$ with the $[P_{66614}]^+$ and $[P_{2228}]^+$ cations. In the inter-molecular region $(q < 2 \text{ Å}^{-1})$, there are pronounced intensity increases in the prepeak and adjacency peak when either anion is paired with the larger cation, combined with a less pronounced increase in peak intensities in the intra-molecular region $(q > 2 \text{ Å}^{-1})$. The prepeak is clearly developed at approximately 0.4 Å^{-1} in the $[P_{66614}]^+$ systems, and the adjacency peak is a single distinctive peak rather than two partially overlapping peaks, as seen in the $[P_{2228}]^+$ systems. These features of the $[P_{66614}]^+$ systems have been observed in the structure functions of other ILs that have the same cation. 8,15 Also, for both anions, the prepeak location shifts to slightly larger q values when comparing $[P_{66614}]^+$ to $[P_{2228}]^+$ ILs. However, saturating the ILs with CO₂ has almost no effect on the structure functions of the $[P_{66614}]^+$ ILs.

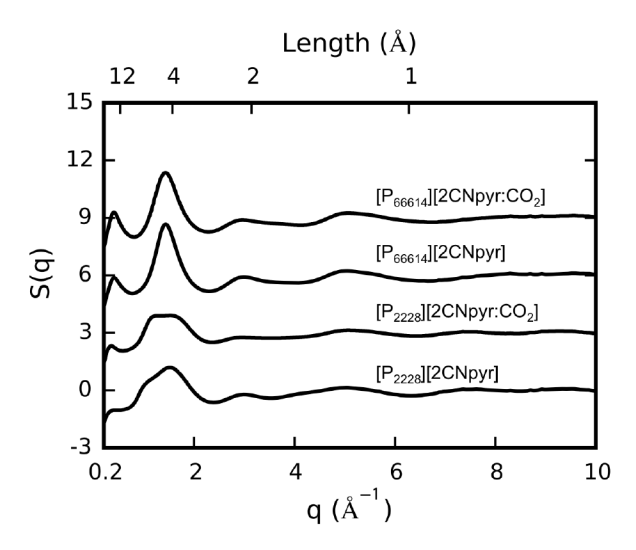


Figure 3: Room temperature (295 K) experimental structure functions for all ILs with [2CNpyr]⁻. The structure functions are offset by 0, 3, 6, and 9 for [P₂₂₂₈][2CNpyr], [P₂₂₂₈][2CNpyr:CO₂], [P₆₆₆₁₄][2CNpyr], and [P₆₆₆₁₄][2CNpyr:CO₂], respectively. The primary abscissa (bottom) is in reciprocal space while the secondary abscissa (top) shows the corresponding real space distance.

The position of the prepeak in S(q) for the two AHA-ILs with the $[P_{66614}]^+$ cation is found at q=0.40 Å⁻¹ and q=0.38 Å⁻¹ for the $[2CNpyr]^-$ and $[4Triaz]^-$ anions, respectivey. Compared to prepeak positions for two other ILs that also have the $[P_{66614}]^+$ cation, this indicates a domain size for the AHA ILs that is between the ones based on Cl^- or $[Tf_2N]^-$ anions. Gontrani et al. reported a prepeak at q=0.37 Å⁻¹ for $[P_{66614}][Cl]^8$, while Kashyap et al. reported a value of q=0.42 Å⁻¹ for $[P_{66614}][Tf_2N]$. ¹⁵ A Cl^- anion for a tetrahedral phosphonium cation should lead to a polar domain with a coordination number of about four anions surrounding each cation, with the size and packing leading to the observed intermediate range order then being determined by nanoscale aggregation of the hydrocarbon tails. The charged head-group interactions for a bulky, flexible anion such as $[Tf_2N]^-$ are necessarily more diffuse. The details of the packing arrangements about the cation for the two AHA anions, $[4Triaz]^-$ and [2CNpyr], must lead to longer-range interactions in $[P_{66614}]^+$ ILs.

A different effect is noted for the position of the prepeak in S(q) for the two AHA

ILs with $[P_{2228}]^+$. The prepeak in S(q) for $[P_{2228}][4\text{Triaz}]$ is observed at q=0.42 Å⁻¹ while there is no well defined prepeak observed for $[P_{2228}][2\text{CNpyr}]$. Previous studies of the liquid structure of $[P_{2228}][Tf_2N]$ showed a prepeak at q=0.4 Å⁻¹ indicating that the packing of this tetraalkylphosphonium cation with the $[4\text{Triaz}]^-$ anion leads to intermediate range order with a less extended range with an effective domain size of about 15 Å, as compared to the domain size of about 16 Å for $[P_{2228}][Tf_2N]$.¹⁷

4.2 Comparison of Experimental and Simulated Structure Functions

A comparison between experimental and simulated densities is shown in Table 1. The simulated densities are consistently lower than the experimental densities by 2-5%, with the difference being larger for ILs with $[P_{2228}]^+$. This level of agreement is sufficient for obtaining reliable liquid structures from MD simulations.

Table 1: Comparison of experimental and simulated densities. Experimental values for all systems other than ILs with unreacted [4Triaz]⁻ have been interpolated based on a linear fit of temperature dependent densities which are included in the SI. All densities are in units of g cm⁻³. Experimental uncertainties are 1×10^{-3} g cm⁻³. Simulation uncertainties in the last significant digit, shown in parenthesis, are estimated using block averaging on the final 2 ns of NPT equilibration.

System	Temperature (K)	Experiment	Simulation	% Difference
$[P_{2228}][2CNpyr]^5$	300	0.953	0.913(1)	-4.2
$[P_{2228}][2CNpyr:CO_2]$	300	1.024	0.977(1)	-4.6
$[P_{2228}][4Triaz]$	313	0.957	0.915(1)	-4.4
$[P_{2228}][4Triaz:CO_2]$	313	1.016	0.979(1)	-3.6
$[P_{66614}][2CNpyr]^4$	300	0.900	0.874(1)	-2.9
$[P_{66614}][2CNpyr:CO_2]$	300	0.929	0.909(1)	-2.2
$[P_{66614}][4Triaz]^4$	313	0.892	0.867(1)	-2.8
[P ₆₆₆₁₄][4Triaz:CO ₂]	313	0.922	0.903(1)	-2.1

The simulated and experimental structure functions for the ILs with $[2\text{CNpyr}]^-$ are shown in Figure 4. Simulated and experimental structure functions for ILs with $[4\text{Triaz}]^-$ are shown in the SI. In all systems, the simulated structure functions have smaller prepeaks than the corresponding experimental structure functions. Additionally, the amplitude of the adjacency peak tends to be slightly larger in the simulations than in the experiments. The simulations capture the experimental observation that the adjacency peak in the $[P_{2228}][2\text{CNpyr}]$ IL broadens upon reaction with CO_2 . Both the experimental and simulated structure functions of the $[P_{66614}]^+$ ILs do not change after reaction with CO_2 . Given the excellent agreement between the simulated and experimental structure functions, the MD structure functions can be partitioned into subcomponents to provide further insights into the liquid structure.

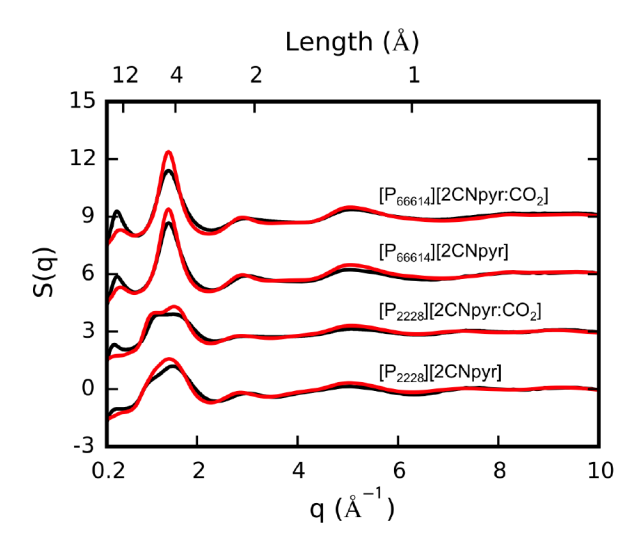


Figure 4: Comparison of experimental and simulated structure functions for all [2CNpyr]⁻ ILs. Experimental structure functions are shown in black. Simulated structure functions are shown in red. The structure functions are offset by 0, 3, 6, and 9 for [P₂₂₂₈][2CNpyr], [P₂₂₂₈][2CNpyr:CO₂], [P₆₆₆₁₄][2CNpyr], and [P₆₆₆₁₄][2CNpyr:CO₂], respectively. The primary abscissa (bottom) is in reciprocal space while the secondary abscissa (top) shows the corresponding real space distance.

4.3 Structure Function Partitioning - Unreacted ILs

Previous work has shown that important IL structure function features can be absent in the experimental structure function due to the cancellation of peaks with antipeaks. The decomposition of the $[P_{2228}][2CNpyr]$ total structure function into the cation-cation $(S^{C-C}(q))$, anion-anion $(S^{A-A}(q))$, and cation-anion $(S^{C-A}(q) + S^{A-C}(q))$ partial structure functions is shown in Figure 5. Both the $S^{C-C}(q)$ and $S^{A-A}(q)$ curves show peaks at a q value of 0.8 Å⁻¹, corresponding to a Bragg domain size of 8 Å. Examination of radial distribution functions shown in the SI confirms that both the cation-cation and anion-anion RDFs have a first maximum at this distance. However, the total structure function does not display a peak at this distance due to a cancellation by the counterion cross correlation antipeak. None of the partial structure functions appear to contribute significantly in the prepeak region. The adjacency peak has contributions from each of the ionic partial structure functions due to the adjacency interactions between each group.

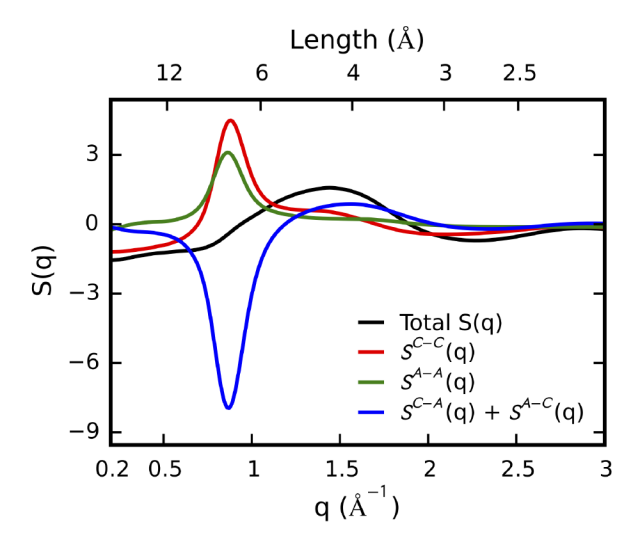


Figure 5: Ionic partial structure functions for $[P_{2228}][2CNpyr]$. The primary abscissa (bottom) is in reciprocal space while the secondary abscissa (top) shows the corresponding real space distance.

It is known that ILs have both polar and nonpolar domains. Following the work of Santos and Kashyap ^{15,32–34}, the partial structure functions were computed by further partitioning **ACS Paragon Plus Environment**

the cation into a polar head group (CH) consisting of the phosphorus and the short alkyl chains and a nonpolar tail group (CT) consisting of the long alkyl chain. Figure 6 shows the resulting partial structure functions involving the CT group. There is indeed a significant contribution to the prepeak from CT-CT correlations. However, this contribution is once again masked from the total structure function due to cancellation by the CT-CH and CT-A antipeaks. Both the CT-CT and CT-A correlations make substantial contributions to the adjacency peak at 1.5 Å^{-1} indicating close contact of these species.

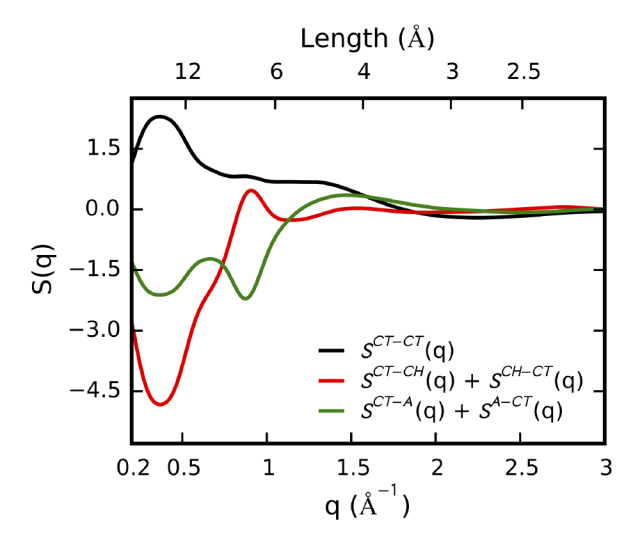


Figure 6: Partial structure functions of $[P_{2228}][2CNpyr]$ involving the CT group. The primary abscissa (bottom) is in reciprocal space while the secondary abscissa (top) shows the corresponding real space distance.

While the structure functions provide useful information about the liquid ordering, they only give a one dimensional description of the three dimensional liquid. Further insight into the arrangement of ions within the IL can be obtained by examining spatial distribution functions (SDFs) from the MD simulations. Figure 7 shows SDFs for the unreacted [P₂₂₂₈]⁺ ILs. Although the structure functions of these ILs are nearly identical, there are stark differences in the SDFs about a central anion. [4Triaz]⁻ has its negative charge distributed more evenly around the aromatic ring while [2CNpyr]⁻ has most of its charge localized on the two nitrogen sites. The different charge distributions cause distinct arrangements of the anions with respect to the cations paragraph and the liquid ordering, they

tends to orient with the nitrogens toward the phosphorus of the cation. The nitrogens attract cation heads, which in turn structure the other anions. The [4Triaz]⁻ anion shows less of a preferred orientation towards the cation where the phosphorus will associate with the entire ring instead of just one side. From the perspective of a central cation, however, the SDFs of the two ILs are quite similar.

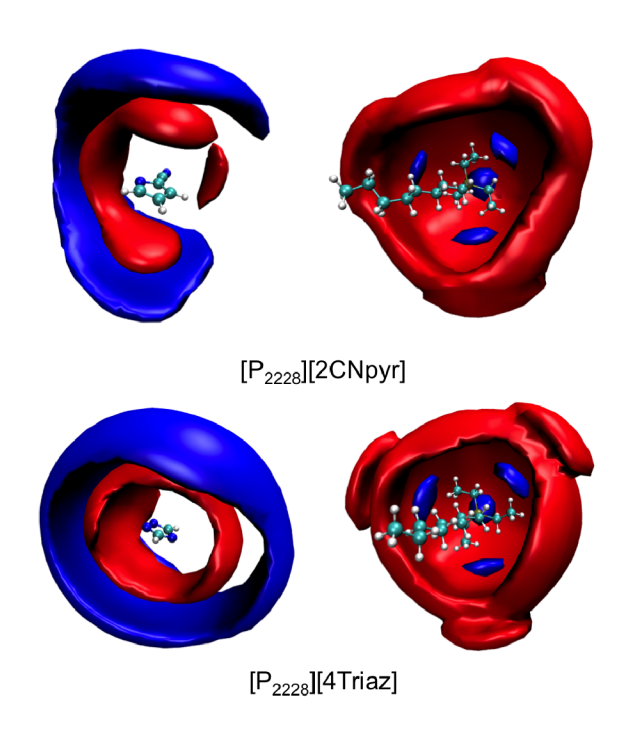


Figure 7: Comparison of SDFs for $[P_{2228}][2CNpyr]$ and $[P_{2228}][4Triaz]$. For the $[P_{2228}][2CNPyr]$ system, the cation P atom (red) is shown at isodensities 5 and 2.4 nm⁻³ and the anion N_1 atom (blue) is shown at isodensities of 2.8 and 7 nm⁻³ for the $[2CNpyr]^-$ and $[P_{2228}]^+$ reference molecules, respectively. For the $[P_{2228}][4Triaz]$ system, the cation P atom (red) is shown at isodensities 5 and 2.5 nm⁻³ and the N_1 atom (blue) is shown at isodensities of 3 and 9 nm⁻³ for the $[4Triaz]^-$ and $[P_{2228}]^+$ reference molecules, respectively. All SDFs were computed using $TRAVIS^{53}$ and rendered using $VMD.^{54}$

4.4 Structure Functions of CO₂-Reacted ILs

While the reaction with CO₂ does not change the main features of the total structure function, there are a few noticeable differences between the unreacted and CO₂-reacted systems. The reaction with CO₂ causes the adjacency peak in the [Property] [2CNpyr] structure function

to flatten and broaden in both the experimental and simulated structure functions. Figure 8 compares the simulation results of the unreacted and CO_2 -reacted total structure function as well as the ionic subcomponents. The peak broadening is a result of several changes in the ionic partial structure functions. Primarily, there is a decrease in the cation-cation and cation-anion correlation in the adjacency peak region. The anion-anion structure function, however, shows no major differences between the unreacted and CO_2 -reacted systems.

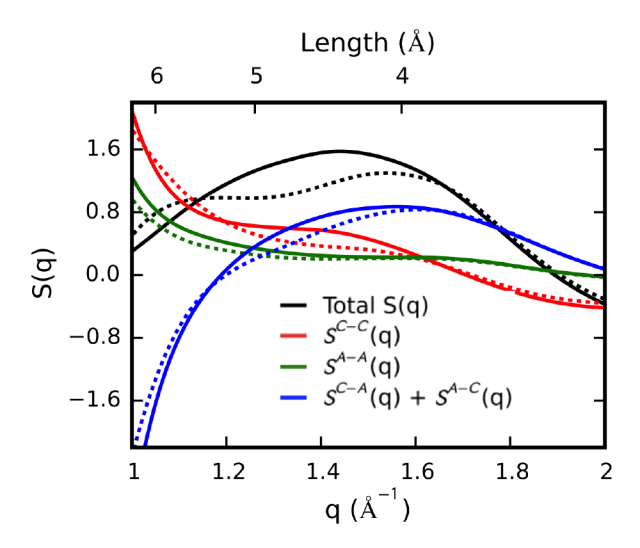


Figure 8: Comparison of unreacted (solid lines) and CO₂-reacted (dashed lines) [P₂₂₂₈][2CNpyr] total structure functions and the ionic subcomponents. The bounds were chosen to highlight the changes in the adjacency peak upon reaction with CO₂. The primary abscissa (bottom) is in reciprocal space while the secondary abscissa (top) shows the corresponding real space distance.

The reaction with CO_2 has even less of an effect on the $[P_{2228}][4Triaz]$ system. Unlike $[2CNpyr]^-$, CO_2 can react at one of two sites on $[4Triaz]^-$ (N_1 and N_3 , noting that N_2 is equivalent to N_1). Figure 9 shows a comparison of the experimental structure function with the simulated structure functions considering the different possible reaction sites of $[4Triaz]^-$. Three different reaction scenarios were considered for this system: all of the CO_2 reacted at the N_1 site, all of the CO_2 reacted at the N_3 site, and a 50/50 mix of the two reaction sites. While all of the simulated structure functions differ slightly from the experimental structure function, they are virtually indistinguishable from one another. This suggests that

the long range order is insensitive to the reaction site of [4Triaz]⁻, and the preferred binding site cannot be determined from the structure functions.

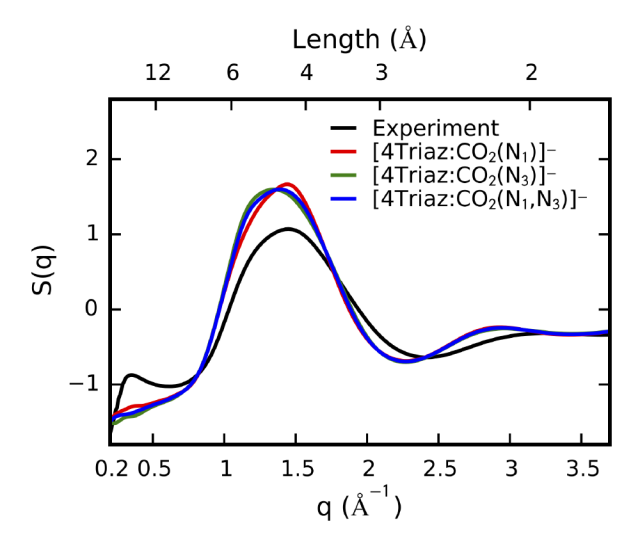


Figure 9: Comparison of experimental and simulated structure functions for $[P_{2228}][4Triaz:CO_2]$. $[4Triaz:CO_2(N_1)]$, $[4Triaz:CO_2(N_2)]$, and $[4Triaz:CO_2(N_1, N_3)]$ correspond to simulations with the CO_2 reacted at the N_1 site, the N_3 site, and a 50/50 mix of the two sites, respectively. The primary abscissa (bottom) is in reciprocal space while the secondary abscissa (top) shows the corresponding real space distance.

The reaction site on $[4\text{Triaz}]^-$ does effect the liquid structure, as shown in Figure 10. When the CO_2 reacts at the N_1 site, the cation interacts primarily with one side of the anion due to the asymmetric charge distribution. When the CO_2 reacts at the N_3 site, however, there is a symmetric charge distribution on the anion and therefore the cation forms close contacts with the entire anion. Similar to the case of the unreacted anions, the SDFs about a central cation show the same four lobes where the anions tend to locate. While the reaction site affects which atom on the anion is closest to the phosphorus of the cation, it does not effect the positions of anions solvating the cation head group. The fact that the cation SDFs show the same behavior regardless of the anion and whether or not it is reacted with CO_2 helps to explain why the structure functions for a given cation display the same characteristic features.

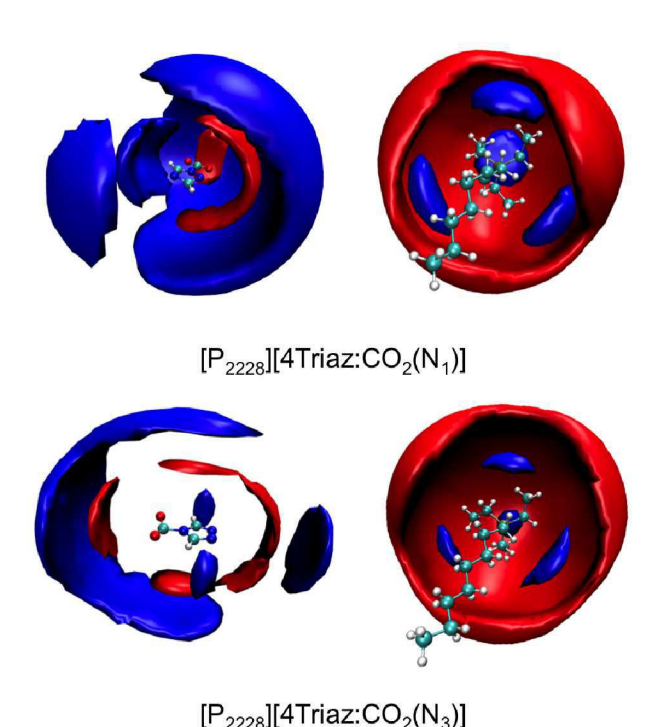


Figure 10: Comparison of SDFs considering the different reaction sites of [P₂₂₂₈][4Triaz:CO₂]. For both of the CO₂-reacted systems, the cation P atom (red) is shown at isodensities of 8 and 2.5 nm⁻³ and the reaction site N atom (blue) is shown at isodensities of 2.5 and 6 nm⁻³ for the [4Triaz:CO₂]⁻ and [P₂₂₂₈]⁺ reference molecules, respectively.

4.5 Structure Function - Cation Substitution

Both experimental and simulation results show that the structure function changes more from cation substitution than from anion substitution. This is to be expected since the maximum spatial extent of the cations is 11 heavy atoms for $[P_{2228}]^+$ and 21 for $[P_{66614}]^+$, while the anions have only 3 or 5 heavy atoms for $[4\text{Triaz}]^-$ and $[2\text{CNpyr}]^-$, respectively. For both anions studied, increasing the cation alkyl chain lengths increases the amplitudes of the prepeak and adjacency peak. Figure 11 shows a partitioning of the $[P_{66614}][2\text{CNpyr}]$ total structure function into its ionic subcomponents. The ionic subcomponents have different behavior than in the $[P_{2228}][2\text{CNpyr}]$ system. Of notable interest is the fact that the cation-cation structure function now has two peaks instead of one and contributes more to the adjacency peak. Additionally, the cation-anion structure function shows a much more well ACS Paragon Plus Environment

defined peak in the adjacency region while the anion-anion structure function makes only a slight contribution to the adjacency peak. The combination of both the cation-cation and cation-anion structuring causes the increase in the adjacency peak as compared to the corresponding $[P_{2228}]^+$ system. Both the cation-cation and anion-anion structure functions show a peak at 0.8 Å⁻¹ while the cation-anion structure function shows an antipeak at this location similar to what was observed for the $[P_{2228}]^+$ cation. However, with the $[P_{66614}]^+$ cation there is a significant left shoulder to the anion-anion peak which, out of all the ionic partial structure functions, makes the largest contribution to the prepeak.

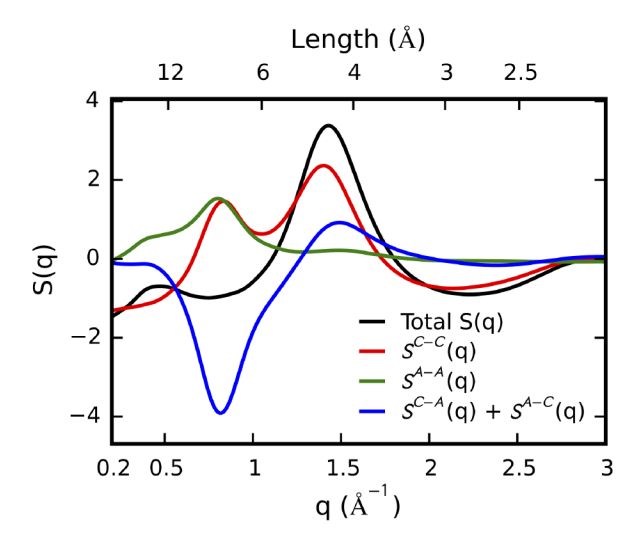
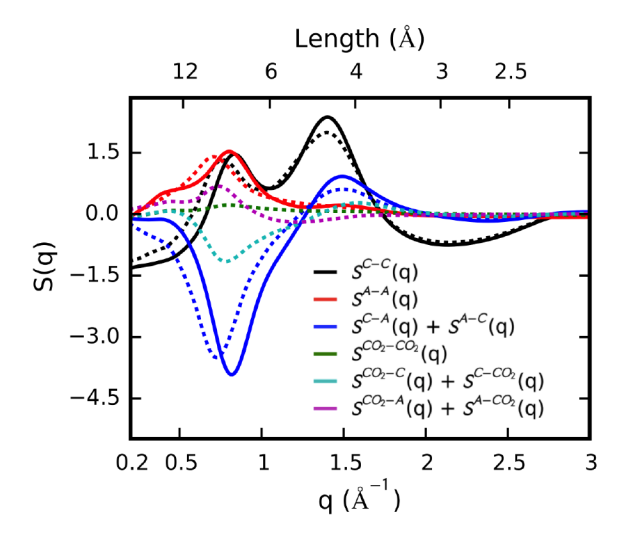


Figure 11: Decomposition of the $[P_{66614}][2CNpyr]$ total structure function into its ionic partial structure function components. The primary abscissa (bottom) is in reciprocal space while the secondary abscissa (top) shows the corresponding real space distance.

The reaction with CO_2 in the $[P_{66614}]^+$ systems does not change the total structure function. However, the ionic partial structure functions shown in Figure 12 have appreciable differences between the unreacted and CO_2 -reacted systems. The anion-anion peak shifts towards smaller q values, which makes sense due to the increased anion size after the reaction. The cation-anion antipeak also shifts to the same q value. The CO_2 - CO_2 partial structure function is rather flat and featureless making a slight contribution to intermolecular features over a wide range of q values. The CO_2 -anion partial structure function has a peak in the charge alternation region as well aroad physical extending to small q values while the

CO₂-cation partial structure function forms an antipeak in the charge alternation region and makes a slight contribution to the adjacency peak. Once again, the experimental structure function provides much useful information regarding ordering of different liquid domains, but correlations of specific species can be "drowned out" due to the panoptic nature of the scattering experiment.



Comparison of unreacted (solid lines) and CO₂-reacted (dashed lines) [P₆₆₆₁₄][2CNpyr] ionic and subionic partial structure functions. The primary abscissa (bottom) is in reciprocal space while the secondary abscissa (top) shows the corresponding real space distance.

Discussion

The AHA ILs studied in this work have the same characteristic structure function features as previously studied ILs: a prepeak, a "hidden" charge alternation peak, and an adjacency peak. The prepeak forms between 0.3 and 0.4 Å^{-1} , depending on the cation, corresponding to a real space distances of 21 and 16 Å, respectively. Charge alternation occurs near 0.8 $\rm \mathring{A}^{-1}$ corresponding to a real space distance of 8 Å, consistent with computed RDFs. There is also an adjacency peak which forms at 1.5 Å^{-1} corresponding to a length of 4 Å. Examination of the SDFs helps to explain the origin of these features. The anions are attracted to the polar ACS Paragon Plus Environment

CH group and they tend to occupy four lobes between the short cation alkyl chains. These anions in turn attract other CH groups forming polar domains within the IL. Likewise, the nonpolar CT group doesn't interact much with either the anions or the CH groups, and tends to aggregate with other CT groups. The formation of the polar and non-polar domains gives rise to features in the structure function. The prepeak results from the alternation of the two domains within the IL. The charge alternation feature, which is absent in the total structure functions, results from the alternation of charged species within the polar domain. The peak at 1.5 Å^{-1} results from a multitude of adjacency interactions within the IL between nearest neighbors such as anions immediately solvating the CH group, aggregated CT groups, and small contributions from cations and anions forming the same solvation shell around an ion.

Comparison of experimental and simulated structure functions of CO_2 -reactive ILs reveals information about the IL landscape. The experimental structure functions are insensitive to the anion because both anions are similar in size, having five membered rings that undergo similar steric interactions within the IL. Both [4Triaz]⁻ and [2CNpyr]⁻ paired with either $[P_{2228}]^+$ or $[P_{66614}]^+$ have structure functions with the same characteristic shapes. However, the ordering lengths are different as determined by the cation.

The structure function doesn't directly reveal the different three dimensional local structure near the anions. [4Triaz] has more observed orientations with respect to the cation than does [2CNpyr]. From the prospective of the cation, however, the two anions behave quite similarly, tending to occupy four high probability lobes between alkyl chains of the CH group. For this reason, both anions end up producing comparable structure functions.

The reaction with CO_2 has little influence on the overall liquid structure function. There is only a slight change in the structure of $[P_{2228}]^+$ ILs upon reaction with CO_2 and there is no change in the structure of $[P_{66614}]^+$ ILs after reaction. The reaction with CO_2 does cause a slight shift in the anion-anion partial structure functions due to the increased anion size. The added CO_2 does change the product anion charge distribution and thus the orientation towards the phosphorus of the cation, but it does not change the product anion solvation of cation head groups enough to change the liquid structure. This supports experimental evidence that the liquid viscosity does not change much after reaction with CO_2 , because the liquid ordering and thus the inter-ionic interactions giving rise to the viscosity don't **ACS Paragon Plus Environment**

change when the anion reacts with CO₂. Furthermore, examination of structure functions for different [4Triaz]⁻ reaction sites shown in Figure 9 demonstrate that the total structure function is completely insensitive to the reaction site.

The most significant change in the liquid structure results from cation substitution. Comparison of the corresponding $[P_{2228}]^+$ and $[P_{66614}]^+$ ILs shows that the increased alkyl chain length on both the CH and CT groups results in increased intensities of both the prepeak and the adjacency interaction peak. Increasing the cation size causes the cation-cation partial structure function to split from one to two peaks. One of the cation-cation peaks remains at the original charge alternation location while the other peak is the primary contributor to the adjacency interaction peak. As the alkyl chain lengths increase, there are increased adjacency interactions between cations as both the CT and CH chains start to aggregate with one another. Additionally, the anion-anion partial structure functions in the $[P_{66614}]^+$ ILs form a broad shoulder at small q values, which contributes significantly to the formation of the prepeak. The cation is the major determinant of the IL structure because it has both polar and nonpolar components causing the IL structure to have two distinct domains. The anions tend to be confined to the same locations near the cation phosphorus atom regardless of the cation size. This well defined structuring of counterions becomes highly pronounced in $[P_{66614}]^+$ ILs because the nonpolar domains are sufficiently large to form continuous percolating networks within the IL.

6 Conclusions

The liquid structure functions of AHA ILs are similar to previously studied ILs. The large size of the cation causes the formation of both polar and nonpolar domains within the IL. The correlated structure of these two domains increases with the cation size and its ability to form continuous nonpolar domains. As such, the cation plays the main role in ordering. The anions are only minor players in the liquid structure as different anions tend to occupy the same preferred locations near the phosphorus between the short alkyl chains of the cation. The organization of the polar domains, therefore, is insensitive to the specific anion and whether or not it has reacted with CO₂. Furthermore, the different reaction sites considered ACS Paragon Plus Environment

on [4Triaz] produce nearly identical structure functions.

The total structure functions of reactive AHA ILs don't change appreciably upon reaction with CO₂. The unreacted and CO₂-reacted anions tend to have the same spatial preference relative to the cation. Both the polar and nonpolar domains remain approximately the same before and after reaction so that the total liquid structure function is not dramatically affected by the reaction. This observation helps to explain why the viscosities of these ILs do not change appreciably upon reaction with CO₂.

While many of the experimental systems exhibit similar one dimensional structure functions, the actual structure within the first solvation shell is sensitive to the anion size and charge distribution. However, these effects fail to manifest distinguishable correlated ordering in the outer solvation shells resulting in the same long range structuring features. The experimental structure function is a good reporter of the ordering length scales but it fails to tell a complete description of the local three dimensional IL liquid structure. MD lends itself to provide further insights in spatial correlations of different species as well as probable orientations of adjacent ions.

Supporting Information

Force field parameterization procedure and all force field parameters, experimental densities of clean ILs and CO₂ saturated ILs, experimental CO₂ solubility data, comparison of simulated [P₂₂₂₈][2CNpyr] total structure functions using 12 and 14 Å cutoffs, comparison of simulated [P₂₂₂₈][2CNpyr] total structure functions for 1000 and 2000 ion pair systems, comparison of [P₂₂₂₈][4Triaz] simulated structures functions at 295 and 313 K, comparison of simulated and experimental structure functions at small q values for [2CNpyr]⁻ ILs, experimental structure functions for [4Triaz]⁻ ILs, comparison of simulated and experimental structure functions at small q values for [4Triaz]⁻ ILs, and RDFs for unreacted and CO₂-reacted [P₂₂₂₈][2CNpyr].

Acknowledgment

Support for the work of QRS and EJM was provided by the Air Force Office of Scientific

ACS Paragon Plus Environment

Research under AFOSR award number FA9550-14-1-0306. Computational resources were provided by the Notre Dame Center for Research Computing. Claudio Margulis and Jeevapani J. Hettige are acknowledged for their help with the structure function calculations. We acknowledge time on beamline 11-ID-B at the Argonne National Laboratory Advanced Photon Source under APS General User Proposal GUP-43233. For experimental support at APS beamline 11-ID-B, we thank Dr. Olaf J. Borkiewicz and Mr. Kevin A. Beyer. EWC was supported by NSF grant number CHE-1362272. JFB and SO acknowledge financial support from the University of Notre Dame Incropera-Remick Fund for Excellence. We thank Samuel Seo for obtaining some of the density data. We thank Boning Wu, Man Zhao, and Jonathan H. Fetherolf for helping with the capillary sealing for some ILs and the data process using the Fit2D and PDFgetX2 programs.

References

- (1) Dupont, J.; de Souza, R. F.; Suarez, P. A. Z. Ionic Liquid (Molten Salt) Phase Organometallic Catalysis. *Chem. Rev.* **2002**, *102*, 3667-3692.
- (2) Hasib-ur-Rahman, M.; Siaj, M.; Larachi, F. Ionic Liquids for CO₂ Capture Development and Progress. *Chem. Eng. and Process.* **2010**, *49*, 313-322.
- (3) Zhang, X.; Zhang, X.; Dong, H.; Zhao, Z.; Zhang, S.; Huang, Y. Carbon Capture with Ionic Liquids: Overview and Progress. *Energy Environ. Sci.* **2012**, *5*, 6668-6681.
- (4) Seo, S.; Quiroz-Guzman, M.; DeSilva, M. A.; Lee, T. B.; Huang, Y.; Goodrich, B. F.; Schneider, W. F.; Brennecke, J. F. Chemically Tunable Ionic Liquids with Aprotic Heterocyclic Anion (AHA) for CO₂ Capture. J. Phys. Chem. B 2014, 118, 5740-5751.
- (5) Seo, S.; DeSilva, M. A.; Xia, H.; Brennecke, J. F. Effect of Cation on Physical Properties and CO₂ Solubility for Phosphonium-Based Ionic Liquids with 2-Cyanopyrrolide Anions. J. Phys. Chem. B 2015, 119, 11807-11814.
- (6) Gurkan, B.; Goodrich, B. F.; Mindrup, E. M.; Ficke, L. E.; Massel, M.; Seo, S.; Senftle, T. P.; Wu, H.; Glaser, M. F.; Shah, J. K.; Maginn, E. J.; Brennecke, J. F.; Schneider, W. F. Molecular Design of High Capacity, Low Viscosity, Chemically Tunable Ionic Liquids for CO₂ Capture. *J. Phys. Chem. Let.* **2010**, *1*, 3494-3499.
- (7) Teague, C. M.; Dai, S.; Jiang, D. Computational Investigation of Reactive to Nonreactive Capture of Carbon Dioxide by Oxygen-Containing Lewis Bases. *J. Phys. Chem.* A 2010, 114, 11761-11767.
- (8) Gontrani, L.; Russina, O.; Celso, F. L.; Caminiti, R.; Annat, G.; Triolo, A. Liquid Structure of Trihexyltetradecylphosphonium Chloride at Ambient Temperature: An X-ray Scattering and Simulation Study. J. Phys. Chem. B 2009, 113, 9235-9240.
- (9) Bhargava, B. L.; Devane, R.; Klein, M. L.; Balasubramanian, S. Nanoscale Organization Room Temperature Ionic Liquids: A Coarse Grained Molecular Dynamics Simulation Study. Soft Matter 2007, 3, 1395-1400.
 ACS Paragon Plus Environment

- (10) Fujii, K.; Soejima, Y.; Kyoshoin, Y.; Fukuda, S.; Kanzaki, R.; Umebayashi, Y.; Yamaguchi, T.; Ishiguro, S.; Takamuku, T. Liquid Structure of Room-Temperature Ionic Liquid, 1-Ethyl-3-methylimidazolium Bis-(trifluoromethanesulfonyl) Imide. *J. Phys. Chem. B* **2008**, *112*, 4329-4336.
- (11) Fukuda, S.; Takeuchi, M.; Fujii, K.; Kanzaki, R.; Takamuku, T.; Chiba, K.; Yamamoto, H.; Umebayashi, Y.; Ishiguro, S. Liquid Structure of N-butyl-N-methylpyrrolidinium Bis(trifluoromethanesulfonyl) Amide Ionic Liquid Studied by Large Angle X-ray Scattering and Molecular Dynamics Simulations. J. Mol. Liq. 2008, 143, 2-7.
- (12) Kanzaki, R.; Mitsugi, T.; Fukuda, S.; Fujii, K.; Takeuchi, M.; Soejima, Y.; Takamuku, T.; Yamaguchi, T.; Umebayashi, Y.; Ishiguro, S. Ion-ion Interaction in Room Temperature Ionic Liquid 1-ethyl-3-methylimidazolium Tetrafluoroborate Studied by Large Angle X-ray Scattering Experiment and Molecular Dynamics Simulations. J. Mol. Lig. 2009, 147, 77-82.
- (13) Hardacre, C.; Holbrey, J. D.; Mullan, C. L.; Youngs, T. G. A.; Bowron, D. T. Small Angle Neutron Scattering from 1-alkyl-3-methylimidazolium Hexafluorophosphate Ionic Liquids (C(n)mim PF6, n=4, 6, and 8). J. Chem. Phys. 2010, DOI: 10.1063/1.3473825.
- (14) Bodo, E.; Gontrani, L.; Caminiti, R.; Plechkova, N. V.; Seddon, K. R.; Triolo, A. Structural Properties of 1-Alkyl-3-methylimidazolium Bis(trifluoromethyl)sulfonylamide Ionic Liquids: X-ray Diffraction Data and Molecular Dynamics Simulations. J. Phys. Chem. B 2010, 114, 16398-16407.
- (15) Kashyap, H. K.; Santos, C. S.; Annapureddy, H. V. R.; Murthy, N. S.; Margulis, C. J.; Castner, Jr., E. W. Temperature-dependent Structure of Ionic Liquids: X-ray Scattering and Simulations. *Faraday Discuss.* **2012**, *154*, 133-143.
- (16) Castner, Jr., E. W.; Margulis, C. J.; Maroncelli, M.; Wishart, J. F. Ionic Liquids: Structure and Photochemical Reactions. *Annu. Rev. Phys. Chem.* **2011**, *62*, 85-105.

 ACS Paragon Plus Environment

- (17) Kashyap, H. K.; Santos, C. S.; Murthy, N. S.; Hettige, J. J.; Kerr, K.; Ramati, S.; Gwon, J.; Gohdo, M.; Lall-Ramnarine, S. I.; Wishart, J. F.; Margulis, C. J.; Castner, Jr., E. W. Structure of 1-Alkyl-1-methylpyrrolidinium Bis(trifluoromethylsulfonyl)amide Ionic Liquids with Linear, Branched, and Cyclic Alkyl Groups. J. Phys. Chem. B 2013, 117, 15328-15337.
- (18) Dhungana, K. B.; Faria, L. F. O.; Wu, B.; Liang, M.; Ribeiro, M. C. C.; Margulis, C. J.; Castner, Jr, E. W. Structure of Cyano-anion Ionic Liquids: X-ray Scattering and Simulations. *J. Chem. Phys.* **2016**, DOI: 10.1063/1.4955186.
- (19) Santos, C. S.; Murthy, N. S.; Baker, G. A.; Castner, Jr., E. W. Communication: X-ray Scattering from Ionic Liquids with Pyrrolidinium Cations. *J. Chem. Phys.* **2011**, DOI: 10.1063/1.3569131.
- (20) Fujii, K.; Kanzaki, R.; Takamuku, T.; Kameda, Y.; Kohara, S.; Kanakubo, M.; Shibayama, M.; Ishiguro, S.; Umebayashi, Y. Experimental Evidences for Molecular Origin of Low-Q Peak in Neutron/X-ray Scattering of 1-alkyl-3-methylimidazolium Bis(trifluoromethanesulfonyl)amide Ionic Liquids. J. Chem. Phys. 2011, DOI: 10.1063/1.3672097.
- (21) Russina, O.; Triolo, A. New Experimental Evidence Supporting the Mesoscopic Segregation Model in Room Temperature Ionic Liquids. *Faraday Discuss.* **2012**, *154*, 97-109.
- (22) Russina, O.; Triolo, A.; Gontrani, L.; Caminiti, R. Mesoscopic Structural Heterogeneities in Room-Temperature Ionic Liquids. *J. Phys. Chem. Lett.* **2012**, *3*, 27-33.
- (23) Hayes, R.; Warr, G. G.; Atkin, R. Structure and Nanostructure in Ionic Liquids. *Chem. Rev.* **2015**, *115*, 6357-6426.
- (24) Urahata, S. M.; Ribeiro, M. C. C. Structure of Ionic Liquids of 1-alkyl-3-methylimidazolium Cations: A Systematic Computer Simulation Study. *J. of Chem. Phys.* **2004**, *120*, 1855-1863.
- (25) Canongia Lopes, J. N. A.; Pádua, A. A. H. Nanostructural Organization in Ionic Liquids. J. Phys. Chem. B. 2996 and D. 2333 Environment

- (26) Atkin, R.; Warr, G. G. The Smallest Amphiphiles: Nanostructure in Protic Room-Temperature Ionic Liquids with Short Alkyl Groups. *J. Phys. Chem. B* **2008**, *112*, 4164-4166.
- (27) Weingärtner, H. Understanding Ionic Liquids at the Molecular Level: Facts, Problems, and Controversies. *Angew. Chem. Int. Ed. Engl.* **2008**, 47, 654-670.
- (28) Russina, O.; Triolo, A.; Gontrani, L.; Caminiti, R.; Xiao, D.; Hines, Larry G., J.; Bartsch, R. A.; Quitevis, E. L.; Pleckhova, N.; Seddon, K. R. Morphology and Intermolecular Dynamics of 1-alkyl-3-methylimidazolium Bis(trifluoromethane)sulfonylamide Ionic Liquids: Structural and Dynamic Evidence of Nanoscale Segregation. J. Phys.: Condens. Matter 2009, 21, 424121.
- (29) Hayes, R.; Imberti, S.; Warr, G. G.; Atkin, R. Pronounced Sponge-like Nanostructure in Propylammonium Nitrate. *Phys. Chem. Chem. Phys.* **2011**, *13*, 13544-13551.
- (30) Hettige, J. J.; Kashyap, H. K.; Margulis, C. J. Communication: Anomalous Temperature Dependence of the Intermediate Range Order in Phosphonium Ionic Liquids. *J. Chem. Phys.* **2014**, DOI: 10.1063/1.4867900.
- (31) Araque, J. C.; Hettige, J. J.; Margulis, C. J. Modern Room Temperature Ionic Liquids, a Simple Guide to Understanding Their Structure and How It May Relate to Dynamics. J. Phys. Chem. B 2015, 119, 12727-12740.
- (32) Hettige, J. J.; Kashyap, H. K.; Annapureddy, H. V. R.; Margulis, C. J. Anions, the Reporters of Structure in Ionic Liquids. *J. Phys. Chem. Let.* **2013**, *4*, 105-110.
- (33) Kashyap, H. K.; Santos, C. S.; Daly, R. P.; Hettige, J. J.; Murthy, N. S.; Shirota, H.; Castner, Jr., E. W.; Margulis, C. J. How Does the Ionic Liquid Organizational Landscape Change when Nonpolar Cationic Alkyl Groups Are Replaced by Polar Isoelectronic Diethers? J. Phys. Chem. B 2013, 117, 1130-1135.
- (34) Kashyap, H. K.; Hettige, J. J.; Annapureddy, H. V. R.; Margulis, C. J. SAXS Antipeaks Reveal the Length-scales of Dual Positive-negative and Polar-apolar Ordering in Room-temperature Ionic Liquids a Chemius Commun. 2012, 48, 5103-5105.

- (35) Santos, C. S.; Annapureddy, H. V. R.; Murthy, N. S.; Kashyap, H. K.; Castner, E. W.; Margulis, C. J. Temperature-dependent Structure of Methyltributylammonium Bis(trifluoromethylsulfonyl)amide: X ray Scattering and Simulations. *J. Chem. Phys.* **2011**, *134*, DOI: 10.1063/1.3526958.
- (36) Hettige, J. J.; Araque, J. C.; Margulis, C. J. Bicontinuity and Multiple Length Scale Ordering in Triphilic Hydrogen-Bonding Ionic Liquids. *J. Phys. Chem. B* **2014**, *118*, 12706-12716.
- (37) Hammersley, A. P.; Svensson, S. O.; Hanfland, M.; Fitch, A. N.; Hausermann, D. Two-dimensional Detector Software: From Real Detector to Idealised Image or Two-theta Scan. *High Pressure Res.* **1996**, *14*, 235-248.
- (38) Hammersley, A. "FIT2D V10.3 Reference Manual V4.0", European Synchrotron Radiation Facility: 1998.
- (39) Brown, P. J.; Fox, A. G.; Maslen, E. N.; O'Keefe, M. A.; Willis, B. T. M. *International Tables for Crystallography* **2006**, *C*, 554-595.
- (40) Qiu, X.; Thompson, J. W.; Billinge, S. J. L. *PDFgetX2*: A GUI-driven Program to Obtain the Pair Distribution Function from X-ray Powder Diffraction Data. *J. App. Crystallog.* **2004**, DOI: 10.1107/S0021889804011744.
- (41) Berendsen, H. J. C.; van der Spoel, D.; Drunen, R. V. Gromacs: A Message-passing Parallel Molecular Dynamics Implementation. *Comp. Phys. Comm.* **1995**, *91*, 43-56.
- (42) Hess, B.; Kutzner, C.; van der Spoel, D.; Lindahl, E. GROMACS 4: Algorithms for Highly Efficient, Load-Balanced, and Scalable Molecular Simulation. *J. Chem. Theory and Comput.* **2008**, *4*, 435-447.
- (43) Pronk, S.; Pll, S.; Schulz, R.; Larsson, P.; Bjelkmar, P.; Apostolov, R.; Shirts, M. R.; Smith, J. C.; Kasson, P. M.; van der Spoel, D.; Hess, B.; Lindahl, E. *Bioinformatics* **2013**, *29*, 845-854.

- (44) Martnez, L.; Andrade, R.; Birgin, E. G.; Martnez, J. M. PACKMOL: A Package for Building Initial Configurations for Molecular Dynamics Simulations. *J. Comp. Chem.* **2009**, *30*, 2157-2164.
- (45) Nos, S. A Unified Formulation of the Constant Temperature Molecular Dynamics Methods. J. Chem. Phys. 1984, 81, 511-519.
- (46) Hoover, W. G. Canonical Dynamics: Equilibrium Phase-space Distributions. *Phys. Rev.* A 1985, 31, 1695-1697.
- (47) Parrinello, M.; Rahman, A. Polymorphic Transitions in Single Crystals: A New Molecular Dynamics Method. J. App. Phys. 1981, 52, 7182-7190.
- (48) Hess, B.; Bekker, H.; Berendsen, H. J. C.; Fraaije, J. G. E. M. LINCS: A Linear Constraint Solver for Molecular Simulations. *J. Comp. Chem.* **1997**, *18*, 1463–1472.
- (49) Hockney, R. W. Methods in Computational Physics.; 1970;
- (50) Potter, D. Computational Physics.; Wiley: New York.
- (51) Darden, T.; York, D.; Pedersen, L. Particle mesh Ewald: An Nlog(N) Method for Ewald Sums in Large Systems. *J. Chem. Phys.* **1993**, DOI: 10.1063/1.464397.
- (52) Allen, M. P.; Tildesley, D. J. Computer Simulations of Liquids.; Oxford University Press: Great Clarendon Street, Oxford, 1987.
- (53) Brehm, M.; Kirchner, B. TRAVIS A Free Analyzer and Visualizer for Monte Carlo and Molecular Dynamics Trajectories. *J. Chem. Inf. Model.* **2011**, *51*, 2007-2023.
- (54) Humphrey, W.; Dalke, A.; Schulten, K. VMD: Visual Molecular Dynamics. *J. Mol. Graph.* **1996**, *14*, 33-38.